Batteries & Supercaps

Research Article
doi.org/10.1002/batt.202100323

Chemistry Europe
European Chemical Societies Publishing

www.batteries-supercaps.org

Special Collection

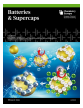

Rational Design of High-Performance Nickel-Sulfur Nanocomposites by the Electroless Plating Method for Electrochemical Lithium-Sulfur Battery Cathodes

Cun-Sheng Cheng[a] and Sheng-Heng Chung*[a, b]

The development of high-performance sulfur-based composite cathodes is a promising strategy to accelerate the reaction kinetics of sulfur and decelerate the irreversible loss of polysulfides. Herein, a strategy for fabricating high-performance metal-sulfur composite cathodes is proposed to achieve a facile synthesis process, adjustable high sulfur content, and excellent electrochemical performance. Electroless nickel plating is applied to achieve a nickel-sulfur nanocomposite with metallic nickel to inhibit the high resistance of the active solid-state materials (*i.e.*, sulfur and lithium sulfide) and the rapid diffusion of the active liquid-state materials (*i.e.*, lithium polysulfides). Therefore, the electroless nickel-plated sulfur (ENS) composite cathode attains high, tunable sulfur contents of 60 wt%–95 wt%, large sulfur loadings of 2–10 mg cm^{-2}, and excellent charge-storage capacity values of 822–1,362 mAh g^{-1}, corresponding to high areal capacity and energy density values of 8.2 mAh cm^{-2} and 17.3 mWh cm^{-2}, respectively.

Introduction

Lithium-ion batteries have come to dominate the energy-storage market due to advancements in battery engineering and the rapid development of energy materials. Continuous improvements in next-generation energy-storage systems promote the lithium-sulfur battery as one of the most promising candidates for energy storage. The lithium-sulfur battery that electrochemically converts between sulfur and lithium sulfide has a high theoretical energy density of 2,600 Wh kg^{-1}. The sulfur cathode, which is both inexpensive and environment-friendly, can generate a high charge-storage capacity approaching 1,675 mAh g^{-1}.[1–4] With such a high capacity, sulfur cathodes are a novel energy-storage technology with the potential to replace lithium-ion battery cathodes, which have a lower charge-storage capacity ranging from 100 to 250 mAh g^{-1}; however, the practical application of sulfur cathodes is restrained by emerging scientific and engineering issues that need to be addressed.[1–5] Sulfur cathode materials inherit the high resistance of sulfur and lithium sulfide (*i.e.*, approximately 10^{-30} and 10^{-14} S cm^{-1}, respectively), which causes low utilization of the active material and a high irreversible capacity loss.[1,6,7] The conversion reaction between sulfur and lithium sulfide involves the formation of lithium polysulfide intermediates, which form a series of active liquid-state materials with the formula of Li_2S_x ($x = 4$–8). The liquid-state polysulfides easily dissolve in the ether-based electrolyte commonly used in lithium-sulfur batteries.[6–8] The dissolved polysulfides, characterized by high reactivity and mobility, diffuse out from the cathode and uncontrollably relocate across the whole cell, leading to unstable electrodes and electrolyte, a quickly fading capacity, and a poor Coulombic efficiency during a short cycle life.[1,6–8] The sluggish redox conversion of the insulating active solid-state materials and the rapid diffusion of the dissolved liquid-state polysulfides lead to issues in engineering battery cathodes with both high sulfur loading and content. Specifically, a low sulfur loading of <2 mg cm^{-2} and an insufficient sulfur content of <60 wt% are often reported in the literature and impede the development of high-energy-density sulfur cathodes, which require both large amounts of sulfur and high electrochemical utilization of these large sulfur amounts.[9–14]

To address the scientific and engineering issues mentioned above, great effort has been devoted to designing and synthesizing various sulfur-based composites, with the goal of using them as cathodes in lithium-sulfur batteries that offer sufficient sulfur loading and high sulfur utilization for technological applications and fulfill the energy density target of 500 Wh kg^{-1}.[14–18] Among the reported sulfur-based composites, carbon-sulfur nanocomposites dominate because of the high conductivity of carbon and the strong polysulfide adsorption of the porous carbon matrix, which improve the charge-transfer capability of the nanocomposite and the adsorption of dissolved polysulfides, respectively.[3,19–23] With the fast development of carbon-sulfur nanocomposites, engineering designs that incorporate polar materials and hierarchical morphologies have been applied to carbon substrates to improve their polysulfide-trapping capability.[19–23] Aside from carbon-sulfur

[a] C.-S. Cheng, Dr. S.-H. Chung
Department of Materials Science and Engineering
National Cheng Kung University
No. 1, University Road, Tainan City 701
E-mail: SHChung@gs.ncku.edu.tw
[b] Dr. S.-H. Chung
Hierarchical Green-Energy Materials Research Center
National Cheng Kung University
No. 1, University Road, Tainan City 701

Supporting information for this article is available on the WWW under https://doi.org/10.1002/batt.202100323

Special Collection An invited contribution to a Special Collection dedicated to Lithium–Sulfur Batteries

nanocomposites, various polymer networks have also been used in synthesizing polymer-sulfur nanocomposites with functional groups that strongly interact with the polysulfide species and thus restrain the dissolution and diffusion of the polysulfides. Moreover, the various synthesis methods of polymers enable unique morphologies with enhanced ionic and electronic conductivities for the composites.[24–26] Ceramics have also been employed as adsorbents and catalysts to retard the migration of polysulfides and retain them within ceramic-sulfur nanocomposites to achieve high retention and conversion of the active material.[27–29] In stark contrast, metallic materials, which feature a higher conductivity than those carbon-sulfur, polymer-sulfur, and ceramic-sulfur host materials, strong polysulfide adsorption capability, and catalytic conversion ability, are rarely reported.[30–35] Moreover, consideration of the engineering design is necessary. One common challenge presented by sulfur-based composite cathodes is the necessity of additional conductive additives and binders. The use of extra inactive material in the composite cathode limits the simultaneous improvement of the sulfur loading and content. Among the aforementioned host materials, metals have the highest density and therefore inhibit the achievement of a high sulfur content in composite and in the cathode. Therefore, metal-sulfur nanocomposites with a high electrochemical utilization and stability must be designed to achieve excellent battery performance in cells with high-loading sulfur cathodes featuring a high sulfur content.[11–14,36,37] In our previous work, the designed nickel-sulfur composite cathode demonstrated improved lithium-sulfur cell performance,[37] which inspires us to explore the details of the composite synthesis. Moreover, the comprehensive understanding of the relationship between composite synthesis and the resulting sulfur cathode electrochemistry and engineering performance would benefit the development of metal-sulfur nanocomposites as various high-energy-density cathode systems.

To achieve this aim, we propose a design for electroless nickel-plated sulfur (ENS) nanocomposites and discuss their engineering applications in lithium-sulfur battery cathodes with both high sulfur contents and loadings. The ENS nanocomposites possess metallic nickel on the surface of the insulating sulfur particles as a result of the reduction of nickel ions during autocatalytic plating.[37–41] By adjusting the synthesis conditions, the ENS nanocomposites attain high sulfur contents in the range of 60 wt%–95 wt%. With electrode engineering, the ENS nanocomposite further realizes increased high sulfur loadings of 2–10 mg cm^{-2}. The high-loading ENS composite cathode demonstrates high electrochemical utilization and therefore attains a high areal capacity of 8.2 mAh cm^{-2} and an energy density of 17.3 mWh cm^{-2} with a stable cyclability for 100 cycles. Our results surpass the required areal capacity for powering electric vehicles (*e.g.*, 2–4 mAh cm^{-2}) and the energy density of commercial lithium-ion battery cathodes (*e.g.*, 10–15 mWh cm^{-2}).[14–18,36] These promising material characteristics are systematically investigated by scanning electron microscopy (SEM) microstructural and elemental analysis, elemental analysis (EA), thermogravimetric analysis (TGA), X-ray diffraction (XRD), and ultraviolet-visible (UV-vis) absorption spectroscopy; the superior electrochemical performances are comprehensively investigated by electrochemical impedance spectroscopy (EIS), cyclic voltammetry (CV), and galvanostatic charge-discharge (GCD) analyses.

Results and Discussion

Electroless nickel-plated sulfur (ENS) nanocomposite: composite synthesis

ENS nanocomposites were synthesized by electroless plating, which plated metal ions on the surface of the substrate through an autocatalytic redox reaction. The autocatalytic reaction mechanism involved the oxidation of the reducing agent in the plating solution, while ionic nickel was reduced to metallic nickel and deposited on the substrate surface with no additional side reactions between the plating metals and the substrates.[38–41] By considering the electrochemical functions of metallic nickel in sulfur cathode chemistry, the ENS nanocomposite was designed with nickel nanoparticles to increase the cathode conductivity and to adsorb the diffusing polysulfides.[30,32]

Figures 1(a–d) illustrates the modified electroless nickel-plating process in synthesizing the ENS nanocomposites. The ENS nanocomposites were prepared with sodium hypophosphite as the reducing agent (*i.e.*, containing $H_2PO_2^-$) and nickel salt as the oxidizing agent (*i.e.*, containing Ni^{2+}) in the plating solution. Because the sulfur substrate is inherently passive (Figure 1a), sensitization and activation reactions were applied to the sulfur particles as pretreatments before the autocatalytic reaction.[38–41] As shown in Figure 1(b), $SnCl_2$ functioned as the sensitizing agent, forming a layer of Sn^{2+}, which was the chemical reducing agent in this process, on the surface of sulfur. As Sn^{2+} readily oxidizes to Sn^{4+} on the surface of sulfur and leads to the reduction of Pd^{2+}, the layer of Sn^{2+} prepares the sulfur for the activation process. The sensitized sulfur particles were subsequently activated by palladium chloride to convert the sensitization sites into nucleation sites, which generated the activated sulfur particles (Figure 1c). This process generates oxidized Sn^{4+} and Pd^0 nuclei on the activated sulfur particles to aid the subsequent nickel plating.[38–40] As shown in Figure 1(d), the pretreated sulfur particles were then subjected to the electroless nickel-plating reaction.[39,40] The electroless nickel-plating reaction was an autocatalysis reaction that involved the reduction of nickel ions by the reducing agent (sodium hypophosphite), as

$$Ni^{2+} + 2H_{ad} = Ni + 2H^+,$$

and the oxidation of sodium hypophosphite, as

$$H_2PO_2^- + H_2O = H_2PO_3^- + 2H_{ad}$$

The full redox reaction was

$$H_2PO_2^- + Ni^{2+} + H_2O = H_2PO_3^- + Ni^0 + 2H^+,$$

Research Article
doi.org/10.1002/batt.202100323
Chemistry Europe
European Chemical Societies Publishing

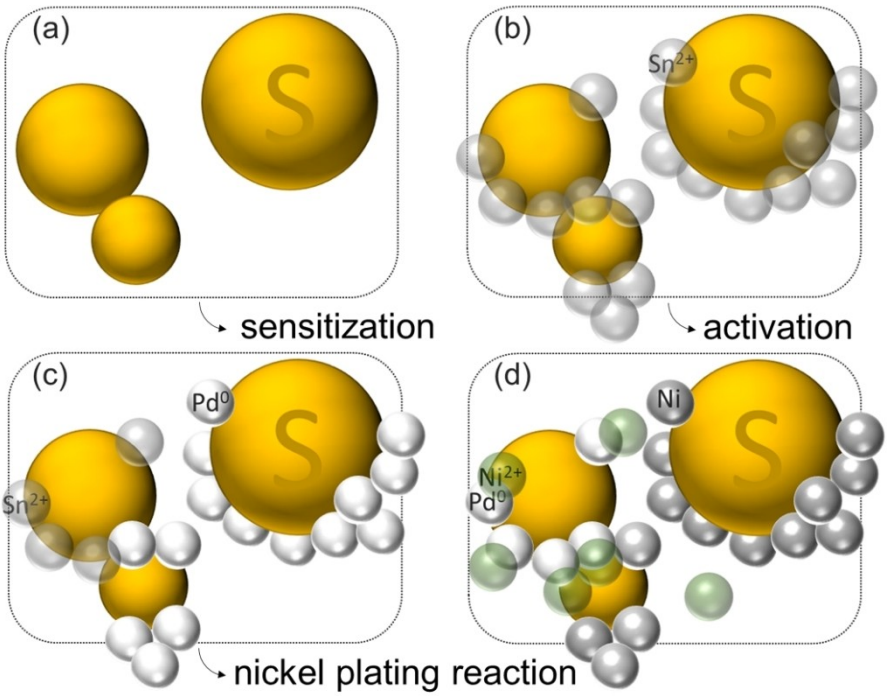

Figure 1. Illustration: synthesis processes of the electroless nickel-plated sulfur (ENS) nanocomposite.

and formed metallic nickel on the sulfur particles as an ENS nanocomposite.[37–41] Although it is known that plated nickel does not undergo a side reaction with sulfur, the amount of nickel plated strongly depends on the formulation and operating conditions of the plating nickel solutions. In this paper, we further study both critical parameters.

The concentration of nickel ions and the plating temperature are known to be the major factors affecting the amount of metallic nickel coating.[38–41] Figures 2(a–c) and (d–f) show the scanning electron microscopy (SEM) microstructural and elemental analysis results for the ENS nanocomposites synthesized with plating nickel solutions with low and high concentrations of nickel ions [*i.e.*, 1 g (6.66 wt%) and 2 g (13.33 wt%) $NiCl_2$ in 15 mL deionized (DI) water], respectively. For each concentration, we also analyzed three different plating temperatures: 70 °C, 80 °C, and 90 °C. High-magnification images of the ENS nanocomposite are shown in Figures S1–S6 in the Supporting Information. The microstructural inspection indicated no obvious morphological differences in the sulfur particles of the ENS nanocomposites. Furthermore, as shown in the microstructural inspection data, the corresponding elemental mapping results, showing the nickel plating (the violet signals) and the original sulfur (the red signals), confirmed that the sulfur particles were successfully plated with nickel. This can be attributed to the two pre-treatments, namely sensitization and activation, which supplied catalysis and nucleation sites to adsorb nickel ions and boost the autocatalysis reduction reaction on the passive sulfur substrate. Moreover, the microstructural/elemental analysis displayed increasingly strong elemental nickel signals as the nickel concentration and temperature of the plating processes increased. This increase in metallic nickel deposition and the fact that the sulfur substrate remained unchanged are consistent with the electroless plating reaction mechanism, which generates a metallic coating as a deposition on the substrate.[39,40] As there were no side effects, the ENS nanocomposites were suitable for use as the active material in a lithium-sulfur battery cathode.

We next conducted systematic elemental and composition analyses to investigate the possible range of sulfur contents of the ENS nanocomposites and identify the most suitable sulfur contents of the ENS nanocomposites for the subsequent electrochemical analysis. Figure 3 summarizes the details of the elemental and composition analyses conducted through energy-dispersive X-ray spectroscopy (EDS), elemental analyzer (EA), and thermogravimetric analyzer (TGA). Figures 3(a and b) indicates that the ENS nanocomposites synthesized under different nickel ion concentrations and plating temperatures attained a high sulfur content ranging between 60 wt% and 95 wt%. After the nickel plating, the EDS elemental analysis suggests that the ENS nanocomposites could be controlled to a low amount of nickel-phosphorus impurity (only 1 wt%–5 wt%). Our low-impurity results confirmed the restricted formation of impurities and nickel-phosphorus alloys and also agreed with previously reported electroless nickel plating methods.[38–41] Figures 3(c and d) illustrates the elemental analysis, which confirmed the adjustable high sulfur content of ~60 wt%–95 wt% for the ENS nanocomposites. The residual content may have resulted from the plated metallic nickel and trace amounts of alloy. As shown in Figures 3(e and f), TGA conducted from room temperature to 500 °C confirmed that the high sulfur contents in the ENS nanocomposites could be well controlled in the range of 60 wt%–95 wt%. As a result, the

Research Article
doi.org/10.1002/batt.202100323
Chemistry Europe
European Chemical Societies Publishing

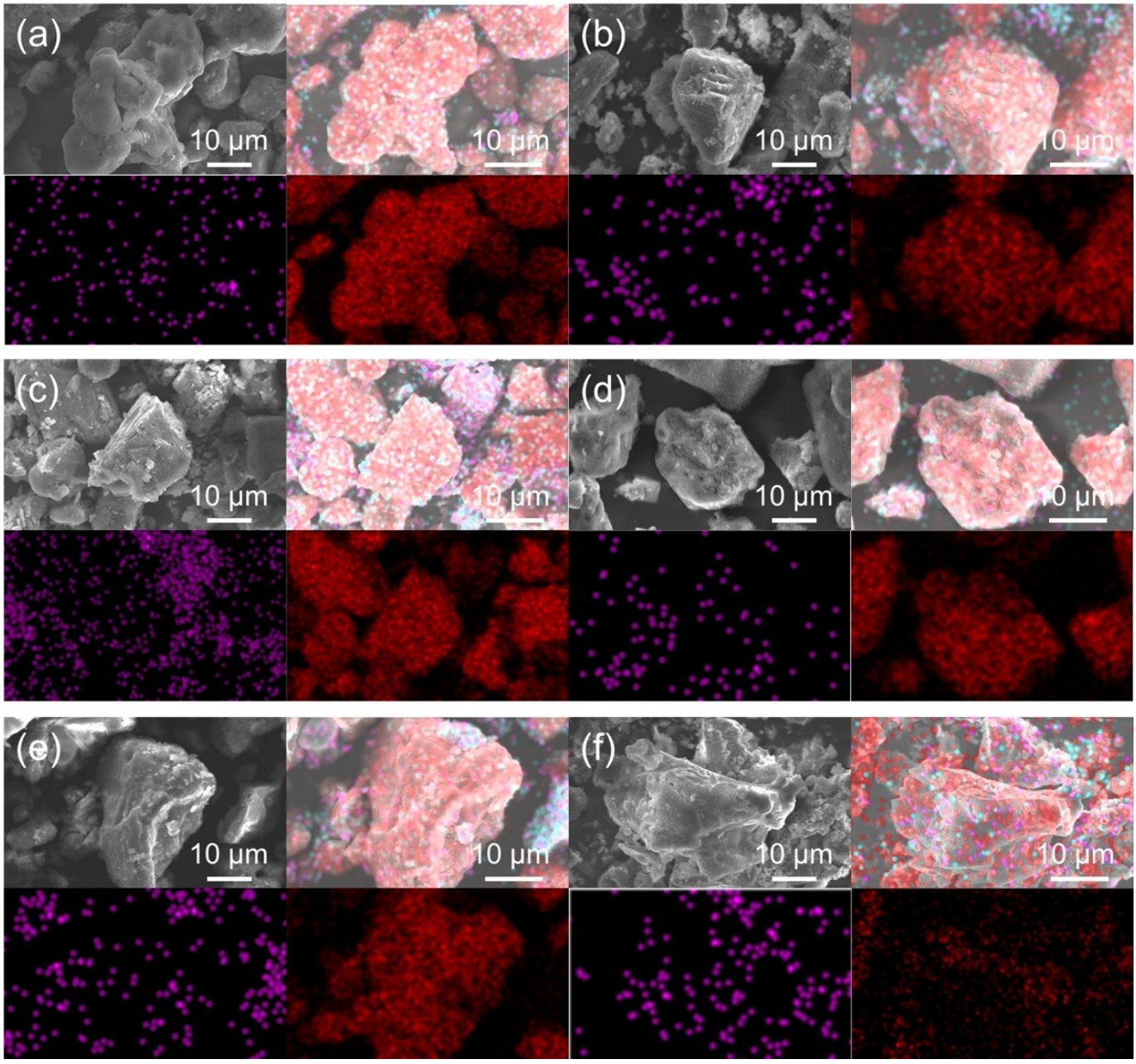

Figure 2. Material characterization: scanning electron microscopy (SEM) microstructural and elemental analysis of ENS nanocomposites synthesized with the low-concentration nickel-plating solution [1 g (6.66 wt%) $NiCl_2$ in 15 mL deionized (DI) water] at a) 70 °C, b) 80 °C, and c) 90 °C and with the high-concentration nickel-plating solution [2 g (13.33 wt%) $NiCl_2$ in 15 mL DI water] at d) 70 °C, e) 80 °C, and f) 90 °C characterized by elemental nickel (violet signals) and elemental sulfur (red signals).

elemental and composition analyses indicated that the autocatalysis plating reaction was promoted with increased temperature, suggesting that strong nickel plating would occur at high temperature (*e.g.*, 90 °C) because a high energy input accelerates the reaction kinetics of autocatalytic plating. However, the further increase of the plating temperature to over 90 °C led to an increasingly volatile plating solution.[39,40] In the tested plating temperature range, we analyzed the composition of the ENS nanocomposites by XRD. As shown in Figure S7, the results support our elemental analysis, as they demonstrate the purity of sulfur in the ENS nanocomposites. Moreover, in Figure S7, nickel peaks can be seen for the sample synthesized using the plating nickel solution with a high concentration of nickel ions. This suggests that nickel was amorphous in the low-concentration sample but crystalline in the high-concentration sample due to its fast nickel-plating reaction.[38–41] The elemental and composition analyses confirmed that 70–90 °C and 6.66 wt%–13.33 wt% were suitable values for the plating temperature and concentration of nickel ions, respectively, to generate ENS nanocomposites with high sulfur contents of 60 wt%–95 wt% and low impurity concentrations. The corresponding analysis values based on different

Research Article
doi.org/10.1002/batt.202100323
Chemistry Europe
European Chemical Societies Publishing

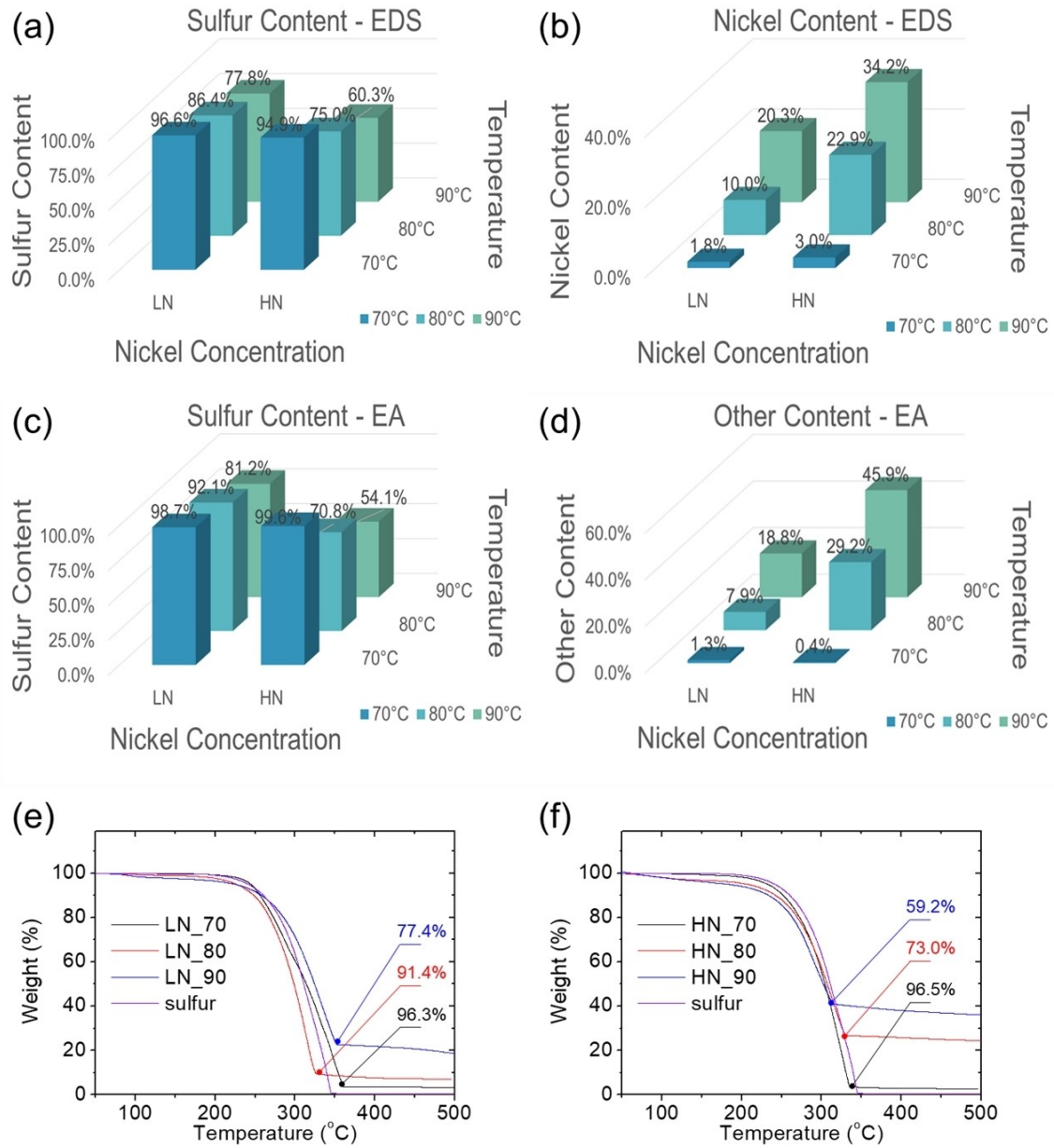

Figure 3. Material characterization: elemental analysis of ENS nanocomposites by a and b) energy-dispersive X-ray spectroscopy (EDS), c and d) elemental analysis (EA), and e and f) thermogravimetric analysis (TGA) (low-concentration nickel-plating solution: LN; high-concentration nickel-plating solution: HN).

analytical methods (*i.e.*, EDS, EA, and TGA) are summarized in Table S1.

Having established the controllability of the sulfur content, we used the ENS nanocomposites with high sulfur contents of 60 wt%, 75 wt%, 85 wt%, and 95 wt% for the subsequent electrochemical analysis. As a control, the reference sample consisted of pure sulfur as the active material. The visible color difference between the ENS nanocomposite powders (*i.e.*, grey-black metallic color) and the reference sulfur sample (*i.e.*, light yellow color) verified the nickel plating on the ENS nanocomposites. The composites with higher sulfur content (*i.e.*, lower nickel content) were lighter in color (Figure S8). The ENS nanocomposites were mixed with liquid electrolyte, and the resulting mixtures of active material and electrolyte were drop-casted onto a regular current collector to form cathodes without the use of additional conductive and binder additives that are needed in conventional sulfur cathode preparation. The cathodes were denoted ENS60, ENS75, ENS85, and ENS95, corresponding to the weight percentage of sulfur in the cathodes. As a control, a reference cathode was also produced with pure sulfur and additional conductive carbon to reach a sulfur content of 60 wt%.

Research Article
doi.org/10.1002/batt.202100323
Chemistry Europe
European Chemical Societies Publishing

Electroless nickel-plated sulfur (ENS) nanocomposite: electrochemistry

Figures 4 and 5 display the results of the electrochemical analysis of the ENS composite cathodes with different high sulfur contents and increasing high sulfur loadings of 2, 6, and 10 mg cm^{-2}. First, Figure 4 shows the electrochemical impedance spectra (EIS). The ENS composite cathodes remained a relatively low cathode resistance when the sulfur content was above 60 wt%. As the sulfur content further increased from 60 wt% to 95 wt%, the cathodes' EIS spectra showed a slight increase in the semicircle diameter at medium frequency, which corresponded to the charge-transfer resistance increasing from 176–297 Ω to 532–609 Ω due to the high resistance of the insulating sulfur.[1–3,7] At low frequency, the spectra of all ENS composite cathodes showed a steep slope, which indicated low lithium-ion diffusion resistance. Therefore, the ENS composite cathode provided an excellent electrochemical environment to promote both the conversion of the active solid-state materials to active liquid-state materials and the subsequent effective electrochemical utilization of sulfur.[1–3,7] Additionally, we found that ENS cathodes with the same sulfur content maintained similar impedances when the sulfur loading was increased three and five times. This implied that the ENS composite was tolerant to application in sulfur cathodes with both high sulfur contents and high loadings, which suggests the outstanding capability in hosting a high amount of sulfur with enhanced utilization.

To support the EIS analysis, Figure 5 shows the cyclic voltammetry (CV) analysis of the ENS composite cathodes. We performed the CV scanning with 5 repeated cycles at each scanning rate and as a function of the scanning rates of 0.03, 0.04, and 0.05 mV s^{-1} for the investigation of the electrochemical reversibility and the redox reaction kinetics, respectively. First, we considered the constant-rate CV curves. At each scanning rate, the high-loading ENS composite cathodes with 6 mg cm^{-2} sulfur and increasing high sulfur contents showed overlapping cathodic peaks and anodic peaks, which indicated high electrochemical reversibility. For the high sulfur content cases (*i.e.*, 75 wt%, 85 wt%, and 95 wt%), the initial CV scan at 0.03 mV s^{-1} showed overlapping CV curves featuring cathodic and anodic peaks that shifted toward high voltage and low voltage, respectively. As a reference, the blue anodic-reaction and the red cathodic-reaction arrows point to the increase of the scanning times. Such CV peak shifts indicated a decrease in cell polarization during cell operation, which is often observed in cathodes with high amounts of active material. Due to the insulating nature of sulfur, high-loading sulfur cathodes often need several cycles of activation to attain high electrochemical utilization.[3,7] After the effective activation in only a few cycles, the high content/loading ENS composite cathodes were characterized by low polarization and an approximately

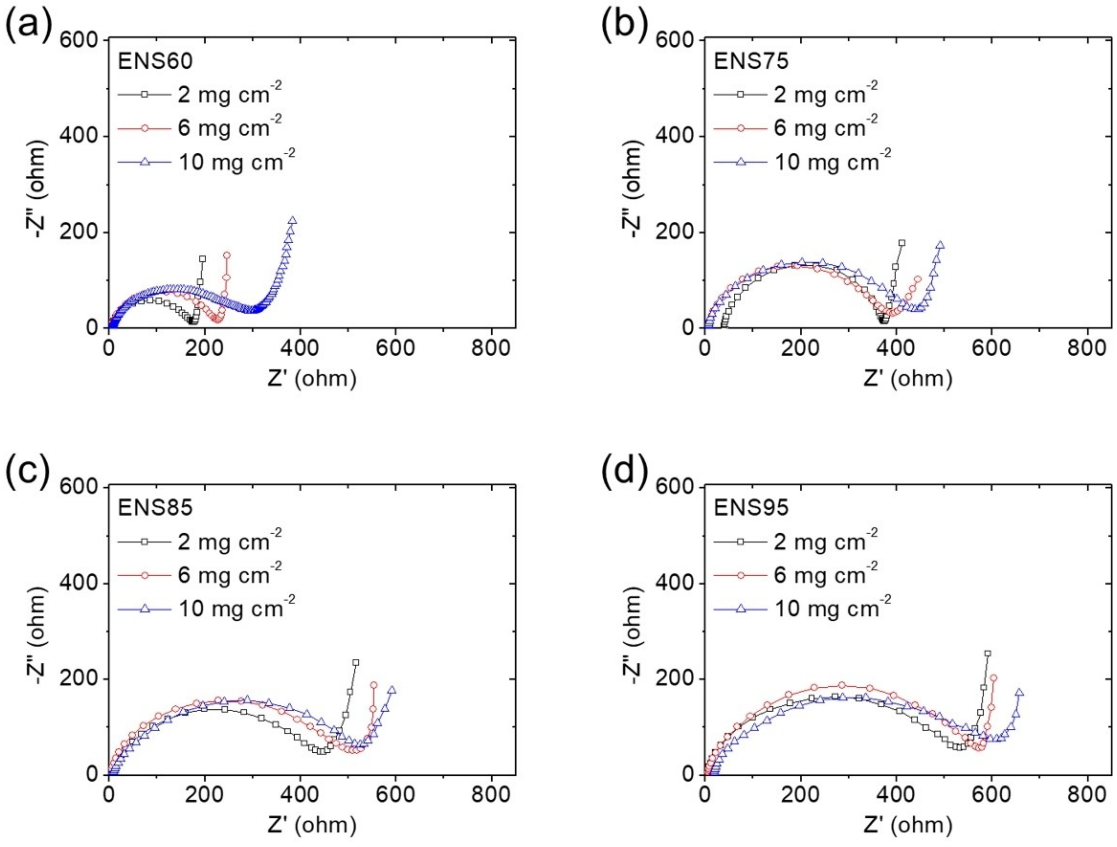

Figure 4. Electrochemical characterization: electrochemical impedance spectroscopy (EIS) analysis of high-loading ENS composite cathodes with high sulfur contents of a) 60 wt%, b) 75 wt%, c) 85 wt% and d) 95 wt%.

Research Article
doi.org/10.1002/batt.202100323
Chemistry Europe
European Chemical Societies Publishing

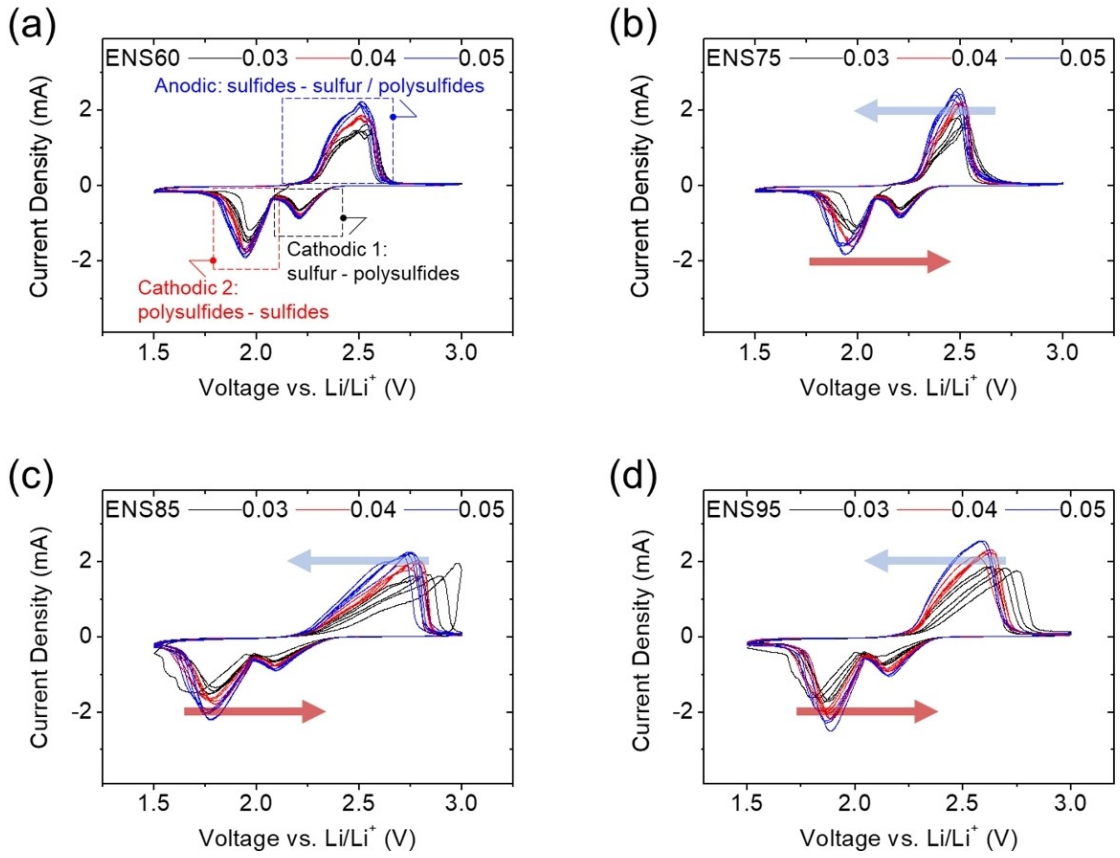

Figure 5. Electrochemical characterization: cyclic voltammetry (CV) curves of high-loading ENS composite cathode with a high sulfur loading of 6 mg cm^{-2} and high sulfur contents of a) 60 wt%, b) 75 wt%, c) 85 wt%, and d) 95 wt% (The inserted cathodic-reaction and anodic arrows show the increase of scanning times).

constant peak current, which demonstrated excellent electrochemical reversibility. In all CV scans, the two overlapping cathodic peaks from 3.0 to 1.5 V indicated a stable discharge reaction from solid-state sulfur to liquid-state polysulfides [represented by cathodic peak 1 (C1)] and from liquid-state polysulfides to solid-state sulfide mixtures [represented by cathodic peak 2 (C2)].[2–4,7] This resulted in a stable discharge capacity during repeated cycling and at various cycling rates. At various scanning rates from 1.5 to 3.0 V, all of the anodic peaks (A) overlapped with each other during continuous scanning, which corresponded to the efficient charge reaction converting sulfides to polysulfides and sulfur.[2–4,7] This efficient charge reaction endowed the high-loading ENS composite cathode with high electrochemical reversibility and efficiency.

Having established the low cathode resistance and high electrochemical reversibility/stability of the ENS composite cathode, we were inspired to explore its ionic transfer characteristics. The lithium-ion diffusion capability of a cathode plays an important role in the conversion of the active material between its solid and liquid states. The rate-dependent CV scans showed well-maintained CV shapes with increasing scanning rates, which confirmed the high reaction kinetics and excellent electrochemical stability. Thus, we further analyzed the peak currents of the cathodic peaks (*i.e.*, C1 and C2) and the anodic peak (*i.e.*, A) at different scanning speeds to calculate the lithium-ion diffusion coefficients of high-loading ENS cathodes with various high sulfur contents (Figure S9).[7,32,36] With the increasing sulfur contents of 60 wt%, 75 wt%, 85 wt%, and 95 wt% in the high-loading ENS cathodes, the lithium-ion diffusion coefficients were 7.2×10^{-8}–9.4×10^{-9}, 7.6×10^{-8}–1.2×10^{-8}, 8.1×10^{-8}–1.3×10^{-8}, and 9.8×10^{-8}–1.5×10^{-8} cm^2 s^{-1}, which indicated that all of the ENS composite cathodes had similarly high lithium-ion diffusion capability (Table S2). The accelerated lithium-ion diffusion kinetics may be attributable to the metallic conductivity contributed by the nickel plating, the catalytic conversion of nickel, and the low electrolyte viscosity caused by the strong adsorption of polysulfides on nickel.[11,27,30,32]

The efficient effect of the ENS nanocomposite in adsorbing polysulfides was analyzed by both the visual color analysis and the ultraviolet-visible (UV-vis) absorption spectroscopy. We prepared a dilute 0.0025 M Li_2S_6 polysulfide solution as the reference. 0.1 g ENS nanocomposites with various sulfur contents were added in the blank solutions. After a static resting of two weeks, the visual color analysis indicated transparent color shown in the polysulfide solutions with ENS nanocomposites, while the blank and reference samples showing brown color of polysulfides (Figure S10). Moreover, the corresponding UV-vis absorption spectroscopy demonstrated limited dissolved polysulfides left in the solutions with

Research Article
doi.org/10.1002/batt.202100323
Chemistry Europe
European Chemical Societies Publishing

ENS nanocomposites; however, strong polysulfide absorption spectroscopy was detected in the solution of blank reference (Figure S11). These analytical results confirm the strong adsorption of polysulfides on the ENS nanocomposite's nickel.

Electroless nickel-plated sulfur (ENS) nanocomposite: cathode engineering

Figure 6 summarizes the battery performance of a reference sulfur cathode and of the ENS composite cathodes with a sulfur loading of 2 mg cm^{-2} and increasing sulfur contents. Figure 6(a) depicts the galvanostatic charge-discharge (GCD) voltage profile of the reference sulfur cathode, which had a sulfur content of 60 wt%. The reversible discharge and charge reactions were consistent with the CV results, featuring a two-step reduction conversion with sulfur to polysulfides at the upper discharge plateau (represented by a black box) and polysulfides to sulfides at the lower discharge plateau (represented by a red box) as well as the reversible oxidation conversion from sulfides to polysulfides and sulfur (represented by a blue box). In the successive cycle, the value of the upper discharge plateau decreased, suggesting the loss of active material resulting from the irreversible diffusion of the

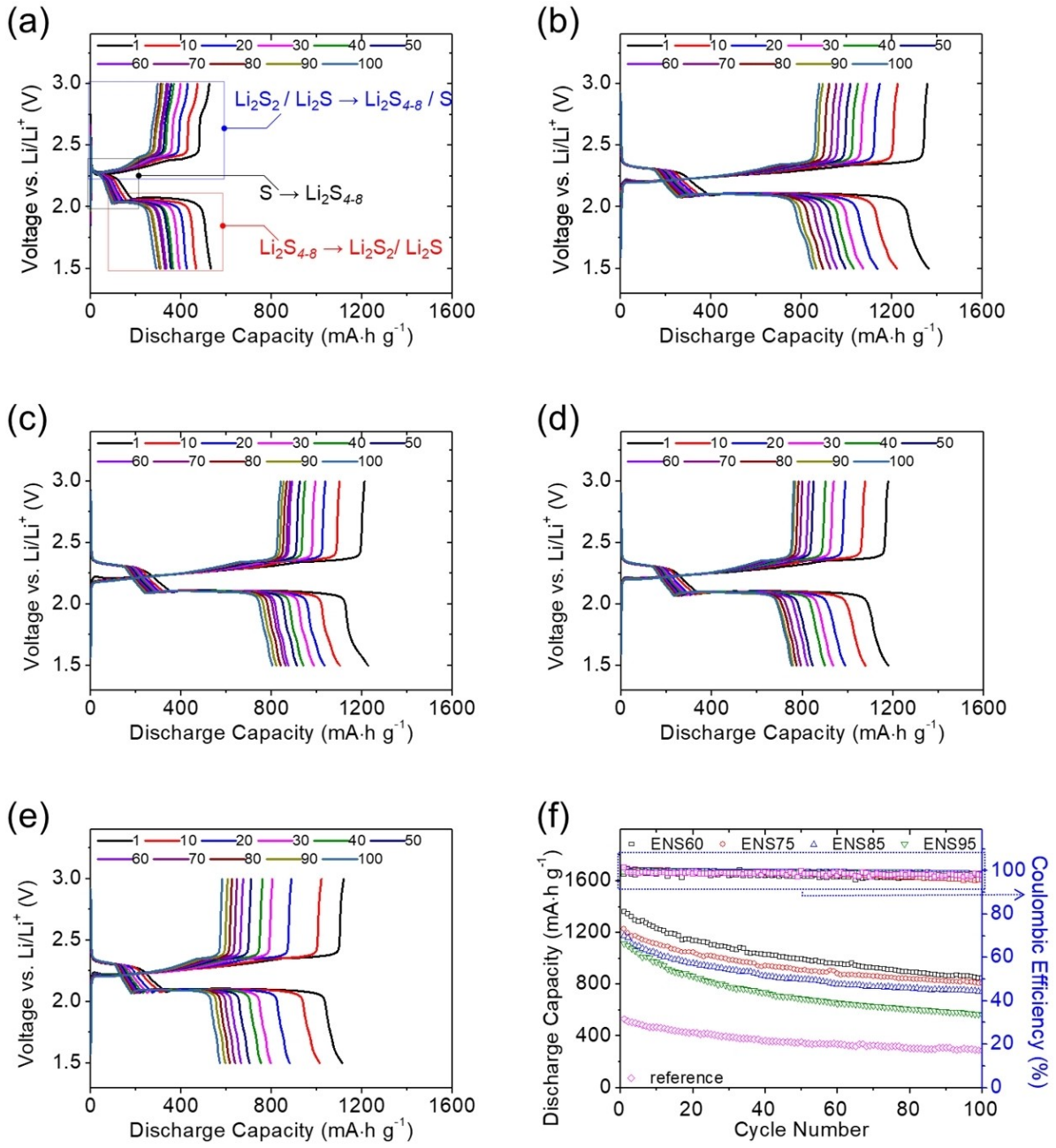

Figure 6. Battery performances: galvanostatic charge-discharge (GCD) voltage profiles of the ENS nanocomposite cathode (2 mg cm^{-2} sulfur): a) reference (60 wt%), b) 60 wt%, c) 75 wt%, d) 85 wt%, and e) 95 wt% sulfur in cathode; and (f) cyclability.

Research Article
doi.org/10.1002/batt.202100323
Chemistry Europe
European Chemical Societies Publishing

dissolved polysulfides out from the cathode, which is the main cause of rapid capacity fade.[7–9] The decline of the lower discharge plateaus indicated the deceleration of the reaction from electrochemically active liquid-state polysulfides to solid-state sulfides. This is associated with the low electrochemical utilization of sulfur cathodes.[7–9,11]

Figures 6(b–e) displays the GCD voltage profiles of ENS composite cathodes with sulfur contents of 60 wt%, 75 wt%, 85 wt%, and 95 wt%, respectively. The profiles exhibit obviously prolonged charge and discharge plateaus with lower voltage hysteresis than the reference shown in Figure 6(a). An overpotential of sulfides converting to polysulfides might result from the limited amount of electrolyte in the cell. However, the following oxidation and subsequent cycling remain stable. This implies that the high efficiency of the reduction and oxidation reactions of the ENS composite cathodes along with their low polarization resulted in a high charge-storage capacity and an excellent efficiency for the discharge/change reaction. As the sulfur content increased, the electrochemical utilization of sulfur remained high, although it fell slightly due to an increase in resistance caused by the insulating sulfur. Nonetheless, all of the cells maintained excellent electrochemical stability. The improved electrochemical utilization (*i.e.*, the reversible high discharge capacity) and the enhanced electrochemical stability

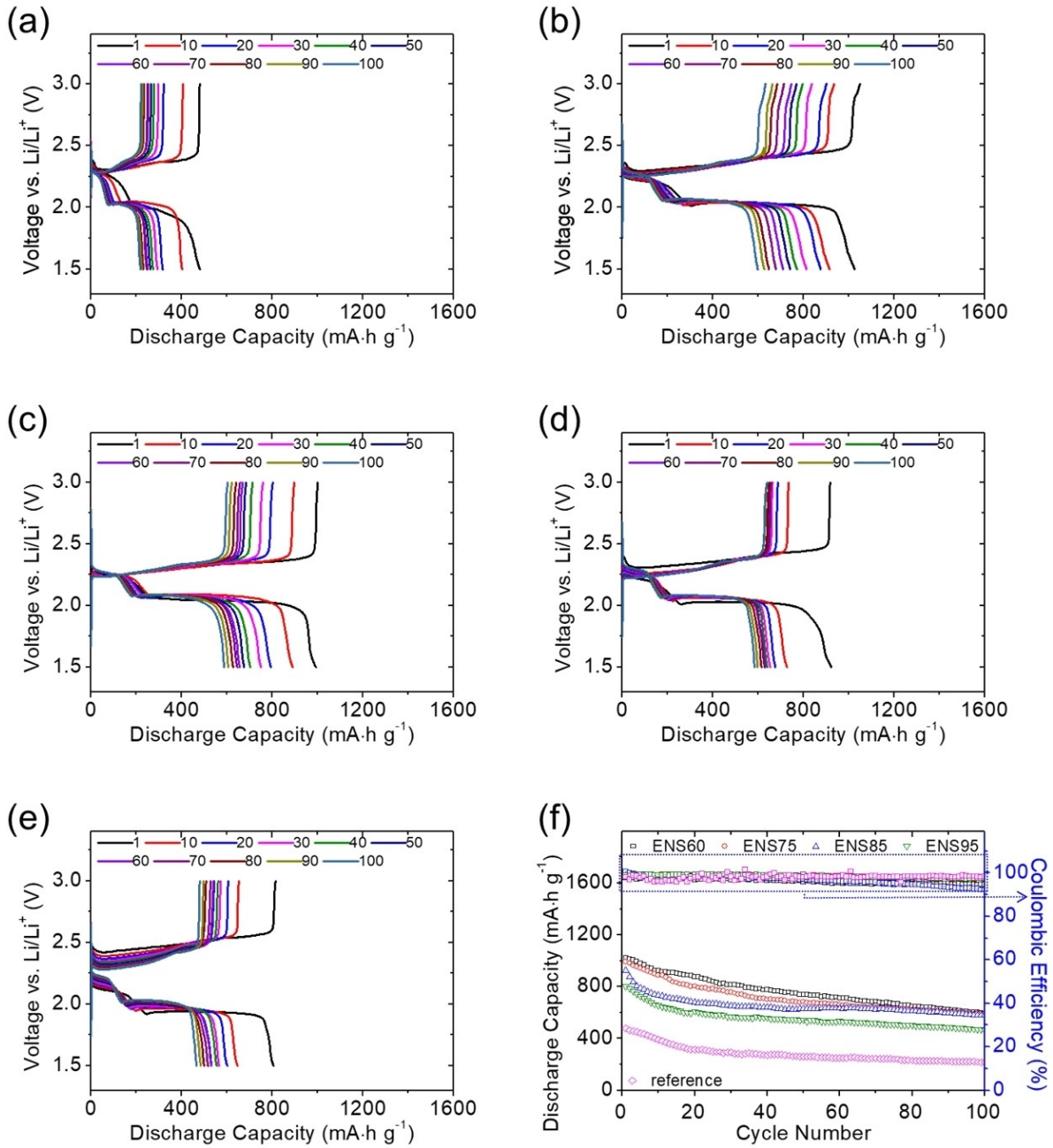

Figure 7. Battery performances: GCD voltage profiles of the high-loading ENS nanocomposite cathode (6 mg cm^{-2} sulfur): a) reference (60 wt%), b) 60 wt%, c) 75 wt%, d) 85 wt%, and e) 95 wt% sulfur in cathode; and f) cyclability.

Research Article
doi.org/10.1002/batt.202100323
Chemistry Europe
European Chemical Societies Publishing

(*i.e.*, the excellent cycle stability and capacity retention) confirmed that the plated metallic nickel in the ENS nanocomposite accelerated the charge-transfer capability and decelerated the active-material loss, which might assist in maintaining the functionality of the nanocomposite and the stability of the cathode.[7,31–35]

Figure 6(f) exhibits the cyclability of the ENS composite cathodes at the cycling rate of C/10. The ENS composite cathodes with high sulfur contents of 60 wt%, 75 wt%, 85 wt%, and 95 wt% attained high discharge capacity values of 1,362, 1,227, 1,180, and 1,113 mAh g^{-1}, respectively. After 100 cycles, the reversible capacities were 848, 806, 745, and 566 mAh g^{-1}, respectively. This indicated that the electrochemical utilization and retention of the ENS composites attained excellent values of 67%–81% and 51%–67%, respectively. At a high cycling rate of 1 C, the ENS composite cathodes with high sulfur contents of 60 wt%, 75 wt%, 85 wt%, and 95 wt% maintained high discharge capacity values of 921, 674, 604, and 564 mAh g^{-1}, respectively (Figure S12). In comparison with the superior electrochemical performance of ENS composite cathodes, the reference sulfur cathode suffered a low peak discharge capacity of 531 mAh g^{-1} and a reversible capacity of only 289 mAh g^{-1} after 100 cycles at the regular C/10 rate and ineffective electrochemical utilization at the fast 1 C rate.

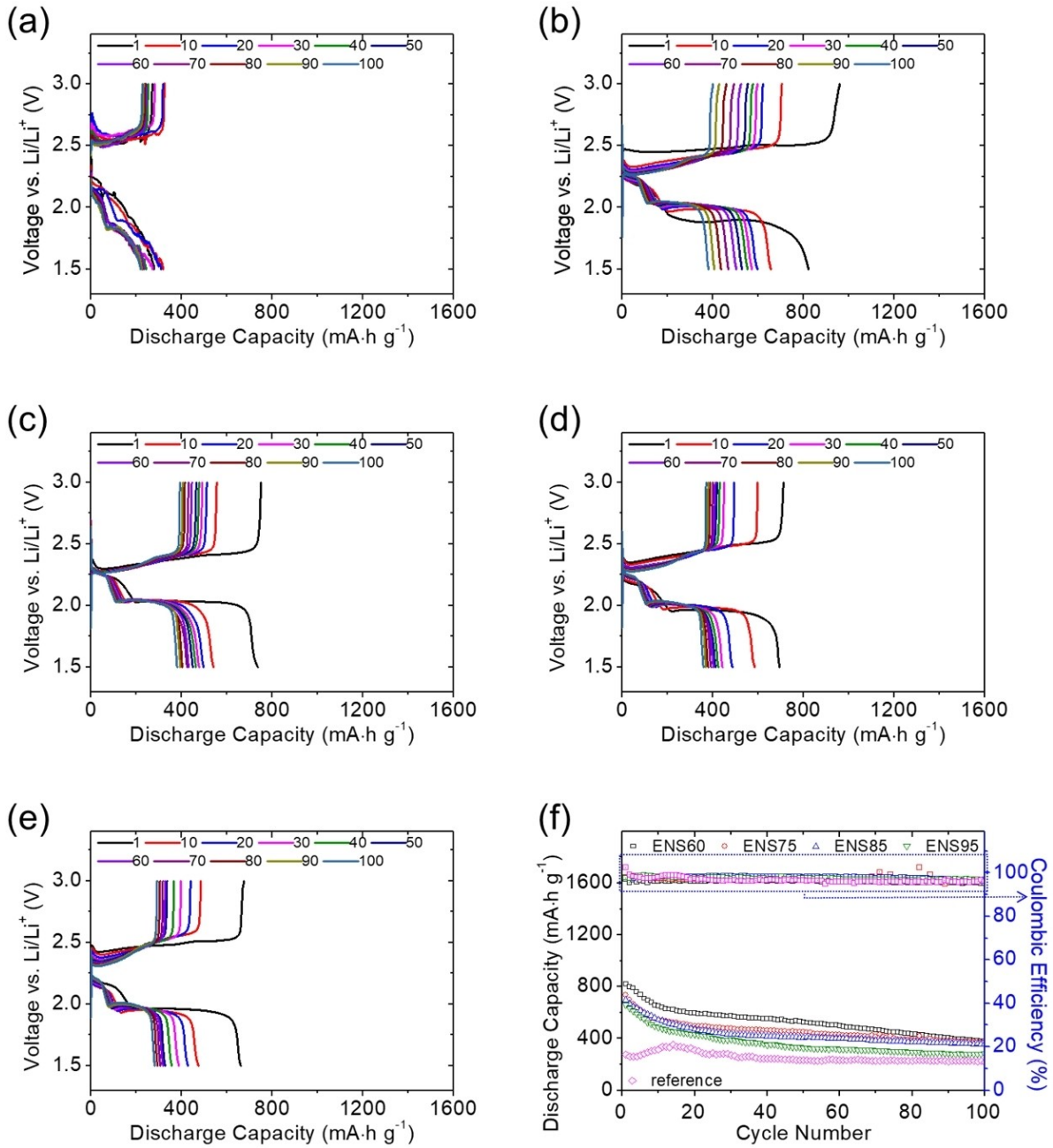

Figure 8. Battery performances: GCD voltage profiles of the ultrahigh-loading ENS nanocomposite cathode (10 mg cm^{-2} sulfur): a) reference (60 wt%), b) 60 wt%, c) 75 wt%, d) 85 wt%, and e) 95 wt% sulfur in cathode; and f) cyclability.

The promising electrochemical characteristics of the ENS composite cathode inspired us to develop a high-loading cathode system. Figure 7 displays the electrochemical performance of the high-loading reference sulfur cathode and the ENS composite cathodes with a high sulfur loading of 6 mg cm^{-2} and high sulfur contents of 60 wt%, 75 wt%, 85 wt%, and 95 wt%. The high-loading reference sulfur cathode with 60 wt% sulfur content suffered a low electrochemical utilization of 28% and high polarization due to the high mass loading of insulating sulfur (Figure 7a). However, for the ENS composite cathodes with the same high sulfur loading of 6 mg cm^{-2}, increasing the sulfur contents from 60 wt% to 95 wt% maintained a high electrochemical utilization of 50%–61% and a low polarization even with a high sulfur content of 95 wt% (Figures 7b–e).

The cyclability shown in Figure 7(f) reveals the importance of adopting the ENS nanocomposites for the engineering development of high-loading sulfur cathodes. The high-loading ENS composite cathodes reached high initial discharge capacity and reversible capacity (in parentheses) values of 1,025 (600), 992 (593), 923 (581), and 805 (472) mAh g^{-1} at sulfur contents of 60 wt%, 75 wt%, 85 wt%, and 95 wt%, respectively, and demonstrated that the resulting high-loading cathodes attained superior electrochemical utilization and high retention of over 60%. As a result of the high sulfur loading and high electrochemical utilization, the ENS cathodes attained high areal capacity and energy density values of 4.8–6.1 mAh cm^{-2} and 10.1–12.9 mWh cm^{-2}, respectively.

With a further increase of the amount of the active material, Figure 8 demonstrates the electrochemical performance of the ultrahigh-loading reference sulfur and ENS composite cathodes with a sulfur loading of 10 mg cm^{-2}. Figure 8(a) confirms that the high amount of sulfur in the cathode caused the reference sulfur cathode to fail to show normal cycling, while Figure 8b affirms the excellent high-loading performance of the ENS composite cathode with the same sulfur content of 60 wt%. Moreover, irrespective of sulfur content, all of the high-loading ENS composite cathodes displayed overlapping and complete upper/lower discharge plateaus and continuous charge plateaus. These positive features confirmed the high electrochemical stability and reversibility of the ENS composite cathodes (Figure 8b–e). Therefore, as shown in Figure 8(f), the high-loading ENS composite cathodes with high sulfur contents of 60 wt%–95 wt% exhibit excellent peak discharge capacity values of 822, 735, 695, and 661 mAh g^{-1}, which correspond to the high areal capacity and energy density of 6.6–8.2 mAh cm^{-2} and 13.9–17.3 mWh cm^{-2}, respectively. Both values are greater than those obtained with oxide cathode materials used in commercial lithium-ion battery cathodes (2–4 mAh cm^{-2} and 10–15 mWh cm^{-2}).[14–18,36]

Conclusion

In summary, we successfully designed and fabricated high-performance electroless nickel-plated sulfur (ENS) nanocomposites to develop lithium-sulfur battery cathodes with a high sulfur amount and a high electrochemical utilization of the active material. The ENS nanocomposites were synthesized by modified electroless nickel-plating, which achieved a high, tunable sulfur content (60 wt%–95 wt%) in the nanocomposites with no unwanted reaction between the functional nickel coating and the sulfur substrate. The plated nickel endowed the ENS nanocomposite with metallic conductivity and polysulfide trapping capability. As a result, the ENS composite cathodes, with no additional conductive or porous additives, attained high charge-storage capacities of 1,113–1,362 mAh g^{-1} and high reversible capacity values of 566–848 mAh g^{-1} after 100 cycles. The resulting fast charge transfer and high active-material retention allowed for the further optimization of the ENS composite with high sulfur loadings of 6 and 10 mg cm^{-2}. The optimal ENS composite cathodes simultaneously attained high sulfur loadings and contents and demonstrated high electrochemical efficiency and stability. Thus, the ENS nanocomposite reached high areal capacity and energy density (*i.e.*, 8.2 mAh cm^{-2} and 17.3 mWh cm^{-2}), outperforming the oxide cathode materials used in commercial lithium-ion battery cathodes (*i.e.*, 2–4 mAh cm^{-2} and 10–15 mWh cm^{-2}). Therefore, our research offers new insights into the rational design of ENS nanocomposites with adjustable metallic plating content and high-energy-density sulfur cathode engineering achieving high sulfur content, loading, and utilization.

Experimental

Composite synthesis of electroless nickel-plated sulfur (ENS)

ENS nanocomposites were synthesized by modified electroless nickel-plating, which consisted of sensitization, activation, and plating reactions. The aim of the sensitization and activation reactions was to form uniform metallic nuclei on the passive substrates to improve the subsequent nickel plating on sulfur.[38–41] The sensitization was performed by mixing 0.1 g stannous chloride ($SnCl_2$, anhydrous, 98%, Alfa Aesar) with 0.4 mL hydrochloric acid (Honeywell FLUKA). The sensitization solution was diluted to 10 mL by deionized (DI) water. Pure sulfur powder (sulfur, 99.5%, Alfa Aesar) was added to the prepared sensitization solution and sensitized for 1 h with continuous stirring. This procedure formed sensitized sulfur powders with a layer of Sn^{2+} ions wrapped around them.[37–40] Activation was conducted by first transferring the sensitized sulfur powders to a 10 mL activation solution prepared with 0.0025 g palladium chloride ($PdCl_2$, 99.9%, Uniregion bio-tech) and 0.025 mL hydrochloric acid. Then, Pd nucleation was used to generate activated sulfur powders.[38–40] The plating process involved two solutions with low and high concentrations of the nickel salt (*i.e.*, nickel chloride, $NiCl_2$). In the low-concentration study, 1 g $NiCl_2$ (anhydrous, 98%, Alfa Aesar) and 1.66 g sodium acetate ($NaOOCCH_3$, anhydrous, 99.0%, Alfa Aesar) were dissolved in 15 mL DI water to form the oxidizing solution, and 2 g sodium hypophosphite ($NaH_2PO_2{\cdot}H_2O$, Alfa Aesar) was dissolved in DI water to form the reducing solution. Each solution was prepared at 70 °C, 80 °C, and 90 °C to test the effect of temperature. The activated sulfur powders were subsequently added to the mixed oxidizing/reducing solutions and stirred for 1 h to conduct the autocatalytic reaction, which generated the ENS nanocomposites. The high-concentration study was conducted in the same manner, but with double the concentrations of the oxidizing and reducing agents. The ENS nanocomposites with sulfur contents of 60 wt%, 75 wt%,

85 wt%, and 95 wt% were synthesized by adopting the corresponding electroless nickel-plating method. The ENS nanocomposite with 60 wt% sulfur was synthesized with high-concentration nickel-plating solution at 90 °C for obtaining the highest nickel content (*i.e.*, the lowest sulfur content). The ENS nanocomposites with 75 wt%, 85 wt%, and 95 wt% sulfur were synthesized with low-concentration nickel-plating solution at 90 °C, 80 °C, and 70 °C, respectively. The sulfur content in each ENS nanocomposite was controlled in a limited low difference of 3 wt%.

Engineering design of the ENS composite cathode

Synthesized ENS nanocomposites with sulfur contents of 60 wt%, 75 wt%, 85 wt%, and 95 wt% were directly blended with liquid electrolyte to form a mixture paste with 1 mg of active material in 10 μL of electrolyte. The electrolyte contained 1.85 M lithium bis(trifluoromethanesulfonyl)imide ($LiN(CF_3SO_2)_2$, 99.995%, trace metals basis, Sigma-Aldrich) dissolved in 1,2-dimethoxyethane/1,3-dioxolane (DME, anhydrous, 99.5% / DOL, anhydrous, 99.8%, Sigma-Aldrich; 55:40 by volume)[42] with 0.2 M lithium nitrate ($LiNO_3$, 99.99%, trace metals basis, Sigma-Aldrich). The mixture paste of ENS nanocomposites and electrolyte was drop-casted onto a commercial carbon-substrate current collector (UNI-ONWARD Corp.) to form the ENS composite cathodes with the electrode area of 1×1 cm^2. The resulting ENS cathode functioned as the working electrode and a lithium foil anode (99.9%, trace metals basis, Sigma-Aldrich) served as the counter electrode in the lithium-sulfur cells, which had sulfur loadings of 2, 6, and 10 mg cm^{-2}. The reference cathode was produced with pure sulfur and Super P carbon (60:40 by weight) and prepared in the same manner as the ENS composite cathode. The resulting reference cathodes have a sulfur content of 60 wt% and increasing sulfur loadings of 2, 6, and 10 mg cm^{-2}.

Material characterization

Scanning electron microscopy was performed using a Hitachi SU-150 scanning electron microscope (SEM) equipped with an energy-dispersive X-ray spectroscope (EDS) to inspect the microstructure and morphology of the ENS nanocomposites, along with their elemental information, using a Bruker Xflash 6–10 energy-dispersive spectrometer. Elemental analysis (EA) was conducted with an Elementar Unicube analyzer, thermogravimetric analysis (TGA) experiments were performed on a PerkinElmer TGA 4000 analyzer with a heating rate of 5 °C min^{-1}, and powder X-ray diffraction (XRD) patterns were recorded by a Bruker D8 DISCOVER diffractometer with Cu K_α radiation to determine the composition and sulfur content of the ENS nanocomposites. Ultraviolet-visible (UV-vis) absorption spectroscopy was performed on a Hitachi U4100 spectrophotometer to identify the polysulfide adsorption capability of the plated nickel in the ENS nanocomposites. The polysulfide adsorption analysis was performed with dilute 0.0025 M Li_2S_6 polysulfide solution that resulted from mixing lithium sulfide and sulfur powders in a molar ratio of 1:5 in the same DME/DOL solvent as the electrolyte preparation and heated at 55 °C for 12 h. 0.1 g various ENS nanocomposites were added in the dilute polysulfide solution as the experimental groups. The blank dilute polysulfide solution and a dilute polysulfide solution with pure sulfur powder were prepared as the blank and reference samples, respectively. These samples were statically rested for two weeks before the visual color and UV-vis analyses.

Electrochemical characterization

Electrochemical impedance spectroscopy (EIS) and cyclic voltammetry (CV) measurements were performed on Biologic VMP-300 and SP-150 electrochemical workstations. EIS was conducted in the frequency range from 1 MHz to 10 mHz with an amplitude of 5 mV to examine the cathode resistance. CV was performed at scanning rates of 0.03, 0.04, and 0.05 mV s^{-1} and with each rate repeated for 5 cycles to analyze the lithium-ion transfer and the electrochemical reversibility, respectively. The lithium-ion transfer was analyzed by calculating the lithium-ion diffusion coefficient with the Randles-Sevcik equation, as $i_{(peak)} = 2.69 \times 10^5 \times \text{concentration}_{(\text{lithium ions})} \times \text{coefficient}_{(\text{lithium ions})}{}^{0.5} \times \text{area} \times \text{rate}^{0.5} \times n^{1.5}$, where $i_{(peak)}$ represents the peak current (A), $\text{concentration}_{(\text{lithium ions})}$ represents the concentration of lithium ions in the electrolyte (mol mL^{-1}), $\text{coefficient}_{(\text{lithium ions})}$ represents the lithium-ion diffusion coefficient (cm^2 s^{-1}), area represents the area of the active electrode (cm^2), rate represents the scanning rate (V s^{-1}), and n represents the charge-transfer number. Galvanostatic charge-discharge (GCD) analyses were conducted at 1.5–3.0 V using Biologic BCS-800 series battery-testing instruments at a cycling rate of C/10. The C/10 rate was selected as the general rate for analyzing the sulfur chemistry for studying both the insulating nature of solid-state active materials and the diffusion issue of liquid-state active materials. The C/10-rate analysis was conducted to investigate the GCD voltage profiles, cyclability, areal capacity, and energy density of the ENS composite cathodes. Additional 1 C-rate analysis was conducted to investigate the high-rate cyclability.

Acknowledgements

This work is supported by the Ministry of Education (MOE) in Taiwan under Yushan Young Scholar Program and the Ministry of Science and Technology (MOST) in Taiwan under grant MOST 110-2636-E-006-012 (Young Scholar Fellowship Program), grant MOST 110-2923-E-006-011, and grant MOST 110-2623-E-006-002. This research was supported in part by Higher Education Sprout Project, Ministry of Education to the Headquarters of University Advancement at National Cheng Kung University (NCKU).

Conflict of Interest

The authors declare no conflict of interest.

Data Availability Statement

The data that support the findings of this study are available from the corresponding author upon reasonable request.

Keywords: Electrochemistry · electroless plating engineering · lithium-sulfur batteries · nanotechnology · sulfur cathode

[1] Q. Zhang, F. Li, J.-Q. Huang, H. Li, *Adv. Funct. Mater.* **2018**, *28*, 1804589.
[2] X. Cheng, T. Hou, K. A. Persson, Q. Zhang, *Mater. Today* **2019**, *22*, 142–158.
[3] Y. Hwa, E. J. Cairns, *ChemElectroChem* **2020**, *7*, 3927.
[4] G. Bieker, V. Küpers, M. Kolek, M. Winter, *Commun. Mater.* **2021**, *2*, 37.
[5] M. Li, J. Lu, Z. Chen, K. Amine, *Adv. Mater.* **2018**, *30*, 1800561.

[6] T. O. Ely, D. Kamzabek, D. Chakraborty, M. F. Doherty, *ACS Appl. Mater. Interfaces* **2018**, *1*, 1783.
[7] M. Wild, L. O'Neill, T. Zhang, R. Purkayastha, G. Minton, M. Marinescu, G. J. Offer, *Energy Environ. Sci.* **2015**, *8*, 3477–3494.
[8] G. Li, S. Wang, Y. Zhang, M. Li, Z. Chen, J. Lu, *Adv. Mater.* **2018**, *30*, 1705590.
[9] M. Zhao, B.-Q. Li, H.-J. Peng, H. Yuan, J.-Y. Wei, J.-Q. Huang, *Angew. Chem. Int. Ed.* **2020**, *59*, 12636.
[10] A. Kilic, Ç. Odabaşı, R. Yildirim, D. Eroglu, *Chem. Eng. J.* **2020**, *390*, 124117.
[11] S.-H. Chung, A. Manthiram, *Adv. Mater.* **2019**, *31*, 1901125.
[12] A. Bhargav, J. He, A. Gupta, A. Manthiram, *Joule* **2020**, *4*, 285–291.
[13] M. Hagen, D. Hanselmann, K. Ahlbrecht, R. Maça, D. Gerber, J. Tübke, *Adv. Energy Mater.* **2015**, *5*, 1401986.
[14] R. Fang, S. Zhao, P. Hou, M. Cheng, S. Wang, H.-M. Cheng, C. Liu, F. Li, *Adv. Mater.* **2016**, *28*, 3374–3382.
[15] J. Xiao, *Adv. Energy Mater.* **2015**, *5*, 1501102.
[16] C. Barchasz, J.-C. Leprêtre, F. Alloin, S. Patoux, *J. Power Sources* **2012**, *199*, 322–330.
[17] J.-Q. Huang, Q. Zhang, H.-J. Peng, X.-Y. Liu, W.-Z. Qian, F. Wei, *Energy Environ. Sci.* **2014**, *7*, 347–353.
[18] D. Lv, J. Zheng, Q. Li, X. Xie, S. Ferrara, Z. Nie, L. B. Mehdi, N. D. Browning, J.-G. Zhang, G. L. Graff, J. Liu, J. Xiao, *Adv. Energy Mater.* **2015**, *5*, 1402290.
[19] J. E. Knoop, S. Ahn, *J. Energy Chem.* **2020**, *46*, 86–106.
[20] S. Li, B. Jin, X. Zhai, H. Li, Q. Jiang, *ChemistrySelect* **2018**, *3*, 2245–2260.
[21] A. Eftekhari, D.-W. Kim, *J. Mater. Chem.* A **2017**, *34*, 17734–17776.
[22] C. Dong, W. Gao, B. Jin, Q. Jiang, *iScience* **2018**, *6*, 151–198.
[23] C.-H. Yu, Y.-J. Yen, S.-H. Chung, *Nanomaterials* **2021**, *11*, 1518.
[24] H. Xiang, N. Deng, H. Zhao, X. Wang, L. Wei, M. Wang, B. Cheng, W. Kang, *J. Energy Chem.* **2021**, *58*, 523.
[25] L. Hencz, H. Chen, H. Y. Ling, Y. Wang, C. Lai, H. Zhao, S. Zhang, *Nano-Micro Lett.* **2019**, *11*, 17.
[26] L.-L. Chiu, S.-H. Chung, *Polymer* **2021**, *13*, 535.
[27] J. Balach, J. Linnemann, T. Jaumann, L. Giebeler, *J. Mater. Chem. A* **2018**, *6*, 23127–23168.
[28] X. Fan, W. Sun, F. Meng, A. Xing, J. Liu, *Green Energy & Environ.* **2018**, *3*, 2–19; Environ. **2018**, 3, 2–19.
[29] Q. Pang, D. Kundu, M. Cuisinier, L. F. Nazar, *Nat. Commun.* **2014**, *5*, 4759.
[30] K. Zhang, F. Qin, J. Fang, Q. Li, M. Jia, Y. Lai, Z. Zhang, J. Li, *J. Solid State Electrochem.* **2014**, *18*, 1025–1029.
[31] N. Mosavati, V. R. Chitturi, L. M. R. Arava, S. O. Salley, K. Y. S. Ng, *Electrochim. Acta* **2015**, *185*, 297–303.
[32] L. Luo, S.-H. Chung, A. Manthiram, *J. Mater. Chem. A* **2017**, *5*, 15002–15007.
[33] V. Marangon, J. Hassoun, *Energy Technol.* **2019**, *7*, 1900081.
[34] V. Marangon, D. D. Lecce, F. Orsatti, D. J. L. Brett, P. R. Shearing, J. Hassoun, *Sustain. Energy Fuels* **2020**, *4*, 2907–2923.
[35] V. Marangon, D. D. Lecce, D. J. L. Brett, P. R. Shearing, J. Hassoun, *J. Energy Chem.* **2022**, *64*, 116–128.
[36] Y.-C. Ho, S.-H. Chung, *Chem. Eng. J.* **2021**, *422*, 130363.
[37] C.-S. Cheng, S.-H. Chung, *Chem. Eng. J.* **2022**, *429*, 132257.
[38] W. J. Crehan, US2690402 A, **1952**.
[39] G. Gutzeit, M. E. T., *KANIGEN* **1956**, *3*, 331–336.
[40] J. G. M. Bremner, *Nature* **1948**, *162*, 183–184.
[41] H. Niederprüm, *Angew. Chem. Int. Ed.* **1975**, *14*, 614–640; *Angew. Chem.* **1975**, *87*, 652–658.
[42] Y. V. Mikhaylik, J. R. Akridge, *J. Electrochem. Soc.* **2004**, *151*, A1969-A1976.

Manuscript received: October 31, 2021
Revised manuscript received: January 3, 2022
Version of record online: January 19, 2022